Tree Physiology 28, 355–366

Fresh-stem bending of silver fir and Norway spruce

TOR LUNDSTRÖM,[1–3] MARKUS STOFFEL[2] and VERONIKA STÖCKLI[1]

[1] *WSL, Swiss Federal Institute for Snow and Avalanche Research SLF, 7260 Davos Dorf, Switzerland*

[2] *Laboratory of Dendrogeomorphology, University of Fribourg, 1700 Fribourg, Switzerland*

[3] *Corresponding author (t.lundstroem@slf.ch)*

Received May 15, 2007; accepted July 24, 2007; published online January 2, 2008

Summary The bending and growth characteristics of large fresh stems from four silver fir (*Abies alba* Mill.) and three Norway spruce (*Picea abies* (L.) Karst.) trees were studied. Twenty logs taken from different stem heights were subjected to four-point bending tests. From the bending test records, we calculated stress–strain curves, which accounted for detailed log taper, shear deformation and self weight. From these curves we determined, among other parameters, the modulus of elasticity (MOE), the modulus of rupture (MOR) and the work absorbed in bending (W). No significant differences were found between species for the wood properties examined. Values of MOE, MOR and W generally decreased with stem height, with MOR in the range of 43 to 59 MPa and MOE ranging from 10.6 to 15.6 GPa. These MOE values are twice or more those reported for stems of young Sitka spruce (*Picea sitchensis* (Bong.) Carr.) trees. Based on the radial growth properties measured in discs from the logs, we calculated predicted values of MOE and MOR for the stem cross section. The predictions of MOE were precise, whereas those of MOR were approximate because of a complex combination of different failure mechanisms. Methods to test and calculate MOE, MOR and W for the stems of living trees are discussed with the aim of improving analyses of tree biomechanics and assessments of forest stability protection.

Keywords: Abies alba, energy absorption, experiment, fresh wood, model validation, nonlinear behavior, Picea abies.

Introduction

Stem bending is an important factor determining tree stability. It occurs as a tree interacts with wind or is subjected to rock impacts or avalanches. The mechanical processes involved during bending and failure of tree stems remain, however, largely unexplored.

Bending stress as a function of bending strain describes how a material behaves while bending, and this function includes several important bending characteristics. For example, the modulus of rupture (MOR) is the maximum value of bending stress, the modulus of elasticity (MOE) represents the secant-modulus of the stress–strain curve, and the work absorbed in bending (W) is proportional to the area under the stress–strain curve. How a stem bends thus depends on its geometry and mechanical properties, which in turn are influenced by radial stem growth processes reflected in annual ring width and knottiness.

The effects of stem growth on the bending properties of dry and sawn wood have been well established by the wood and timber industry. In contrast, how growth affects the mechanical properties of fresh wood, especially of intact tree stems, is less well known (Lundström et al. 2007). The structure of wood in the stem is anisotropic and heterogeneous, with variation in stiffness and strength properties (Trendelenburg and Mayer-Wegelin 1955, Green et al. 1999). Because lumber is sawn in such a way as to minimize heterogeneity in mechanical properties within a piece, we can expect a more complex distribution of stresses during the bending of an entire fresh stem than of dry and sawn wood, and thus different bending stress–strain behaviors. Tests of fresh logs of young Sitka spruce (*Picea sitchensis* (Bong.) Carr.) growing in plantations in Scotland (Cannell and Morgan 1987) with an MOE of about 8 GPa show that cambial age positively influences the cross-sectional MOE. For intact stems of older trees, however, there seems to be no information on MOE or on stem bending in general.

Differences among Norway spruce (*Picea abies* (L.) Karst.) and silver fir (*Abies alba* Mill.) in mechanical bending properties of dry timber are related to growth patterns, not species (Trendelenburg and Mayer-Wegelin 1955, Kucera and Gfeller 1994). To assess possible differences in mechanical properties between these species, data are required on the properties of radial growth that have a significant influence on tested mechanical values.

When tree stems in nature are subject to bending, they react with a combination of mechanisms and modes of failure (e.g., Mattheck and Breloer 1994). Diverse behavior makes it difficult to predict the consequences of stem bending. In static bending tests in the laboratory, shearing or torsion can be limited or accounted for. The shear strain can be calculated (e.g., Newlin and Trayer 1956) and the torsion avoided by selecting straight and round test logs. Independently of how the bending properties of intact stems are tested, a detailed description of stem taper under bark is required, because the determination of MOE, MOR and W depends on measured woody stem diame-

ter in the fourth, third and second power, respectively. It is difficult to predict these properties, because little is known about how the cross-sectional bending stress develops with increasing strain, even for dry and clear wood (Adjanohoun et al. 1998, Dinwoodie 2000).

To assess how mature fresh stems bend and to relate this bending to properties of radial growth, we carried out static, four-point bending tests on 20 logs of silver fir and Norway spruce taken from different stem heights and analyzed radial growth in the laboratory. We present novel data relating to the bending stress–strain of the stem and results from performance tests of models that predict stem bending based on properties of radial stem growth.

Materials and methods

Trees and logs

The stems analyzed for their bending and cross-sectional growth were cut from three large Norway spruce (*P. abies*) and four large silver fir (*A. alba*) trees. These trees grew in a mixed, single-story forest stand of Norway spruce, silver fir, Scots pine (*Pinus sylvestris* L.) and common beech (*Fagus sylvatica* L.) on nearly flat ground. The stand is located on the Swiss Plateau (47°14′ N, 8°53′ W, 460 m a.s.l.) and was previously studied by Lundström et al. (2007). The seven test trees were codominant or dominant in relation to their neighboring trees, straight in stature and apparently healthy. Their bark thickness at breast height relative to the woody stem radius at this height was 6 ± 1%. Further tree data are given in Table 1. Symbols used in this paper are summarized in Table A1.

The trees were felled in mid-November. Before the stems were transported to the laboratory, the stem base was removed to minimize taper, and the upper crown was removed to avoid irregular stem growth due to branching. In the laboratory, the stems were cut into two, three or four sections, depending on the total stem length, resulting in 11 silver fir and nine Norway spruce logs. We measured log length, log diameter at five points along the log axis and mean bark thickness at both ends. Cross sections of the logs were almost perfectly circular. The 20 logs originated from stem heights of between 1.0 and 26.8 m (Table 2).

Table 1. Properties of the four silver fir (*Abies alba*) and three Norway spruce (*Picea abies*) trees subjected to bending tests: AGE = cambial age measured at 1.3 m stem height; H = total tree height; DBH = diameter at breast height; S = slenderness = H/DBH; and L_{cr} = crown length, measured from lowest green branches to top of tree.

Tree	AGE (years)	H (m)	DBH (mm)	S	L_{cr}/H
Silver fir					
1	80	35.0	410	85	0.42
2	75	31.0	400	78	0.40
3	105	33.0	440	75	0.42
4	95	31.5	420	75	0.42
Norway spruce					
5	100	35.0	420	83	0.43
6	80	37.0	415	89	0.43
7	100	31.5	420	75	0.35

Bending tests

One week passed between tree falling and log testing, during which time the stems were kept outside in the shade, fully supported on the ground, to prevent loss of humidity. The fresh logs were subjected to four-point bending tests according to the German industry code, DIN 52186 (DIN 1992), with an exception made for their higher water content. The test geometry followed the European code EN 408 (CEN 2003), with a total span of 5.92 m for logs from Stem heights 1 and 2 (Table 2) and 4.80 m for logs from Stem heights 3 and 4, and a distance between the two symmetrically applied forces of 2.15 and 1.42 m, respectively. The test equipment comprised Parker Hannifin hydraulic cylinders 8201-5500-H021A (HYDREL, Romanshorn, Switzerland) and displacement sensors TK-100-E-2 (PRECISOR Messtechnik, Munich, Germany), and data were acquired at 1 Hz with a Darwin DA 100 (YOKOGAWA Electric, Tokyo, Japan) controller. To avoid local de-

Table 2. Dimensions and height positions of Logs 1–4 of each silver fir (*Abies alba*) and Norway spruce (*Picea abies*) test tree: L_{tot} = total log length; D_c = log diameter at its center; and z_c/H = height of log center relative to total tree height. Log numbers 1–4 are found at Stem heights 1–4, respectively, which refer to ranges of z_c/H.

Tree	Log 1			Log 2			Log 3			Log 4		
	L_{tot} (m)	D_c (mm)	z_c/H	L_{tot} (m)	D_c (mm)	z_c/H	L_{tot} (m)	D_c (mm)	z_c/H	L_{tot} (m)	D_c (mm)	z_c/H
Silver fir												
1	6.85	319	0.19	6.96	288	0.41	5.55	254	0.56	–	–	–
2	6.96	322	0.14	6.90	282	0.40	5.55	242	0.57	–	–	–
3	6.89	353	0.15	7.08	319	0.38	5.57	279	0.54	–	–	–
4	6.15	320	0.26	6.12	273	0.50	–	–	–	–	–	–
Norway spruce												
5	6.45	340	0.13	7.08	307	0.34	5.60	276	0.49	–	–	–
6	6.92	332	0.16	6.95	295	0.37	5.45	254	0.53	5.50	217	0.65
7	6.94	334	0.16	6.96	285	0.38	–	–	–	–	–	–

formation and concentration of stresses perpendicular to the wood grain, each log was placed on a 250-mm-thick, cylindrically sawn veneer board positioned on an articulated joint on each support. For the same reason, both points of load application were provided with cylindrical "gloves" and additional rubber inlays. The load was applied at a constant deflection rate, so that the maximum force was obtained within 120 ± 30 s. The tests were then continued until the logs failed. The load records could be followed until the load returned close to zero. In contrast, the stem deflection could not be recorded (only visually estimated) until the log fell apart, because of the restricted measuring range of the displacement sensors. However, this has no practical implications for the parameters that are the focus of this study.

Growth properties of log cross sections

After the bending tests, 150-mm-long cross sections were cut close to the failure zone of the logs and annual ring width (RW) and knottiness (Q) from pith to bark were measured with a caliper (Figure 1). Based on SIA (2003), we defined Q at the radius from the pith (r) as an eighth of the summed surface area of knots (A_{knots}) intersecting with the 150-mm-long cylinder:

$$Q(r) = \tfrac{1}{8} A_{knots} \in \underbrace{\int_{z-75}^{z+75} \int_{\phi=0}^{2\pi} r\,\phi\, d\phi\, dz}_{\text{cylinder}} \quad (1)$$

where ϕ is the rotation around the z-axis and z is in mm. For comparison, the frequently used knot area ratio (KAR; SIA 2003) applied to our logs approximately equals the mean of $Q(0 \le r \le D_0/2)$, where D_0 is stem diameter under bark. The woody stem discs were weighed to determine disc density.

Water content (u) was not measured in the radial direction and only coarsely in the longitudinal direction (one stem disc per log). We therefore adopted the same distribution for u in the relative radial and longitudinal directions as for the Norway spruce stem growing in the same stand studied by Lundström et al. (2007), and verified that this assumption was correct based on measured disc density. The sapwood and heartwood extensions (Figure 1), which are used only as an approximate description of the radial positions, were estimated on the basis of RW(r) and the RW(r) and $u(r)$ measurements by Lundström et al. (2007). Bark density at testing was an estimated 600 kg m^{-3} (USDA 1972, Schmidt-Vogt 1991).

Analysis

In the analysis of mechanics, we refer to tree coordinates z and x, where z is along the stem with $z = 0$ at the stem base of the standing tree and x is in the direction of deflection with $x = 0$ at the stem center. We also refer to some calculation algorithms that are included in the Matlab 7.0 (MathWorks) software package.

When analyzing the bending behavior of logs, we accounted for log taper, self weight and deflection due to shear forces. The taper of each stem (Table 2) was first given a continuous description with a polynomial fit $D(z)$ based on the diameters measured along the stem. Each fit was then reduced for bark thickness $b(z)$, i.e., $D_0(z) = D(z) - 2b(z)$, where $b(z)$ is a polynomial based on relative bark thickness at breast height, as described by Laasasenaho et al. (2005), which was verified with the bark measurements at each log end.

The bending properties of the logs were characterized based on curves of bending stress (σ) as a function of the bending strain (ε), from zero load to failure. To obtain the $\sigma(\varepsilon)$ curves, we followed seven calculation steps (Table 3) and used two equations (Equations 2 and 3):

$$\begin{aligned} \sigma &= \sigma_F + \sigma_g \\ \sigma_F &= \frac{F D_{0c}}{8 I_{0c}}(L - L_F); \qquad I_{0c} = \tfrac{1}{64}\pi D_{0c}^{\,4} \\ \sigma_g &= \frac{m g D_{0c} L}{16 I_{0c}}; \qquad m = \rho_w V_0 + \rho_b V_b \end{aligned} \quad (2)$$

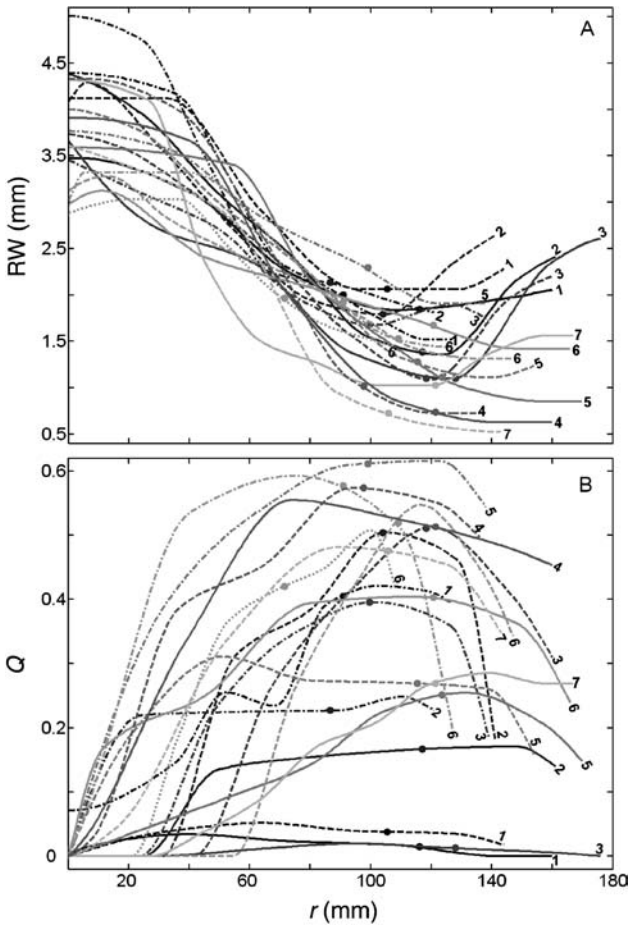

Figure 1. (A) Annual ring width (RW) and (B) knottiness (Q) as functions of radial distance from the pith (r) of logs from silver fir (*Abies alba*) and Norway spruce (*Picea abies*) trees. Each log is identified by tree number (1–7) and linetype: solid = Log 1; dashed = Log 2; dash-dotted = Log 3; and dotted = Log 4. Filled circles indicate approximate locations of heartwood–sapwood borders.

Table 3. Successive steps in analyzing the properties of the bending mechanics of tested logs.

Step	Description
1	Calculation of bending stress (σ; Equation 2), including contributions from applied force and log weight. Maximum σ, independent of type of failure, corresponds to MOR.
2	Calculation of the elasticity in bending E_F (Equation 3; DIN 52 186) due to the applied force F, accounting for shear deformation and detailed log taper.
3	Combination of Steps 1 and 2 into the bending strain $\varepsilon_F = \sigma_F/E_F$ and $E_F(\varepsilon_F)$. As E_F is elasticity in bending corrected for shear deformation, ε_F is bending strain as it would be under pure bending conditions.
4	Calculation of bending strain due to weight of the log: $\varepsilon_g = \sigma_g/E_{0.4F_{max}}$, where $E_{0.4F_{max}}$ is E_F at 40% of maximum F.
5	Concatenation of $(\varepsilon,\sigma) = (0,0)$, (ε_g,σ_g) and (ε_F,σ_F), into the array $\sigma(\varepsilon_E)$, where $E(\varepsilon_E)$ is the corresponding elasticity in pure bending.
6	Definition of MOE as $E(\varepsilon_E)_{0.4MOR}$, i.e., the gradient of the straight line between $\sigma(\varepsilon_E) = 0$ and $\sigma(\varepsilon_E) = 0.4MOR$, and in addition, as $E(\varepsilon_E)_{LIN}$, the gradient for the visually estimated first linear part of $\sigma(\varepsilon_E)$.
7	Computation of $\sigma(\varepsilon)$, where ε is apparent strain, from $\varepsilon = 0$ until the end of the test, with no correction for shear deformation (ε is slightly greater than ε_E). Apart from the analysis of MOE (Step 6), $\sigma(\varepsilon)$ is used throughout the study.

where σ_F is bending stress due to the applied force (F), σ_g is bending stress due to the weight of the log (mg), subscript c refers to the center of the log, I_{0c} is moment of inertia about the log center excluding bark, L is log span (distance between the two supports), L_F is the distance between the two points of load application, m is mass of the log within the span reduced for overhang at the two log ends, g is earth gravity, ρ_w and ρ_b are the bulk densities of fresh wood and bark, respectively, and V is total volume within the span reduced for overhang of the two log ends; and:

$$\begin{aligned} E_F &= \frac{F}{s}\left(\frac{C_1}{48 I_{0c}} + C_2\right) \\ C_1 &= \tfrac{1}{2}(2L^3 - 3L{L_F}^2 - {L_F}^3) \\ C_2 &= \beta\left(\frac{E(z)}{G(z)}\right)' \frac{L}{A_0(1+\tfrac{1}{2}KL)} \end{aligned} \tag{3}$$

where E_F is explained in Table 3, C_1 is a length factor, C_2 is a correction factor for shear deformation and measured difference in diameter under bark (0) between the thin end (1) and the thick end (2) of the log at the supports, with $KL = (D_{02} - D_{01})/D_{01}$ (Cannell and Morgan 1987), β is a load coefficient, which equals 16/81 in four-point bending (Newlin and Trayer 1956), and $(E(z)/G(z))'$ is an estimated ($'$) relationship between the elasticity in bending E and shear G along the grain of the cross section. This relationship depends primarily on the value of E/G at the stem heights where the largest bending strain (in the outermost stem) and shearing strain (in the stem center) occur. Both E and G of fresh wood are correlated with RW (Kollmann 1968, Lundström et al. 2007). For the stems tested, RW in the outermost stem decreased with z, but RW in the stem center remained nearly constant with z, suggesting $(E(z)/G(z))'$ decreases with z. We therefore estimated $G(z)$ in the heartwood and $E(z)$ in the sapwood on the basis of $RW(x,z)$ and adopted $(E(z)/G(z))' = 25 - 0.07z/H$ for all the logs. The contribution of bark to the bending resistance of the log was ignored, because both the shear resistance of the bark-to-wood layer and the shear and bending strength of bark are much lower than the corresponding values of the underlying wood for hardwood species (Einspahr et al. 1984). We believe that these orders of magnitude apply to the softwood species tested. To explore the influence of differences in diameter at the thin and thick log ends and of shear deformation on the calculated MOE values (cf. Table 3), E_F was calculated by setting K and C_2, respectively (Equation 3), equal to zero.

Idealized stress–strain curves were calculated for each bending test, and characteristic bending stress–strain curves were established for the lowest three logs. "Idealized" as used here means that the stress–strain curve includes one ideal elastic and one ideal plastic deformation, and "characteristic" refers to the mean stress–strain curve of the group according to height or species. For details on the calculation methods, see Lundström et al. (2007).

Shear stress as a function of radial distance from the pith and position along the log ($\tau(x,z)$) was calculated as:

$$\tau(x,z) = \frac{4T(z)}{3A_0(z)}\sqrt{1-\left(\frac{x}{\frac{1}{2}D_0(z)}\right)^2} \tag{4}$$

where $T = dM/dz$ is the transverse force along the log (commonly called the shear force), occasioned by the applied forces and the weight of the log, A_0 is the cross-sectional area of the log and $0 < x < D_0/2$. This equation is a simplification, because it assumes the shearing elasticity (G) is constant across the log section. The shear strength ($\tau_{max}(x,z)$; Equation 5) was estimated according to Kollmann (1968) and Dinwoodie (2000) on the basis of the dry wood density ($\rho_0(x,z)$; Equation 6) calculated according to Lundström et al. (2007):

$$\tau_{max}(x,z) = a_1\rho_0(x,z) + a_2 \tag{5}$$

$$\rho_0(x,z) = a_1\log\big(\mathrm{RW}(x,z)\big) + a_2 \tag{6}$$

where $\vec{a} = [0.019\ \ -4.9]$ in Equation 5 and $\vec{a} = [543\ \ -106]$ in Equation 6.

The work absorbed by the logs in bending up to MOR (W_{MOR}) was calculated from the load-deflection curve $F(s)$ as:

$$W_{\mathrm{MOR}} = \tfrac{1}{2} F_g s_g + \int_{s_g}^{s_{\mathrm{MOR}}} F(s)\, ds; \qquad F_g = \tfrac{5}{8} mg \tag{7}$$

where s_g is the initial deflection at mid-span due to the linear load caused by the log weight, s_{MOR} is the total deflection at mid-span at MOR and F_g is the concentrated (fictive) force that causes the same deflection as the log weight. Here, s_g is calculated using MOE.

The numerical values of W_{MOR} were first compared among the logs by dividing their W_{MOR} by the woody volume of the log within the bending span (V_0). General comparisons of W_{MOR} or W_{MOR}/V_0 obtained by this method assume normalized test set-ups, e.g., three-point bending of a beam of a square section according to DIN (1992). Because this was not the case, we: (1) define work as the integral of the stress–strain curve of the tested section, $\int \sigma(\varepsilon)\, d\varepsilon$; and (2) calculate work absorbed by a bent member based on $\int \sigma(\varepsilon)\, d\varepsilon$ according to the methods in the Appendix. The results for W_{MOR} from Equation 7 and from (2) were compared. The work-related material-property completeness (η) was also calculated from the $F(s)$-curve:

$$\eta = \frac{W_{F_{\max}}}{(F_g + F_{\max}) s_{F_{\max}}} \tag{8}$$

where $F_{\max}$ is the maximum applied force, $W_{F_{\max}}$ is the work absorbed by logs in bending due to $F_{\max}$, $s_{F_{\max}}$ is the mid-span deflection due to $F_{\max}$, and $\eta = 1.0$ and 0.5 characterize materials with ideal-plastic and ideal-elastic stress–strain behaviors, respectively.

Experimental values of MOE and MOR of the mid-span cross sections were compared with the calculated predicted values, as proposed by Lundström et al. (2007). These calculated values are obtained in two steps.

In Step 1, reference is made to one cylindrical shell of the cross section in the log mid-span, located at stem height z (cf. Table 2) and at radial position j, where j ranges from pith ($j = 1$) to bark ($j = n$) every 1 mm. The measured data of radial growth are first interpolated radially every mm and then attributed to this shell, of which $\mathrm{MOE}(z)_j$ and $\mathrm{MOR}(z)_j$ are computed as regressions:

$$\mathrm{MOE}(z)_j = a_1 \log\left(\mathrm{RW}(z)_j\right) + a_2 u(z)_j + a_3 \tag{9}$$

$$\mathrm{MOR}(z)_j = a_1 \log\left(\mathrm{RW}(z)_j\right) + a_2 Q(z)_j^2 + a_3 \tag{10}$$

where $\bar{a}$ = [–5860 –25.0 15100] in Equation 9 and $\bar{a}$ = [–17.3 –36.0 66.4] in Equation 10. The standardized regression coefficients, which indicate the impact of each explanatory variable on the response variable, are $\bar{\boldsymbol{a}}$ = [–1.61 –0.49] and $\bar{\boldsymbol{a}}$ = [–1.78 –0.24], respectively, where, for example, $\boldsymbol{a}_2 = a_2 \mathrm{SE}(u)/\mathrm{SE}(\mathrm{MOE})$ for the regression coefficient of u in Equation 9.

In Step 2, values of $\mathrm{MOE}(z)_j$ and $\mathrm{MOR}(z)_j$ obtained in Step 1 are superposed radially, cylindrical shell by shell (j) to form the log section. For MOE, this is described as:

$$\mathrm{MOE}(z)_{\mathrm{sect}} = \frac{\gamma_{\mathrm{MOE}}}{x_n(z)^4} \sum_{j=1}^{n} \mathrm{MOE}(z)_j \left(x(z)_{j+1}^4 - x(z)_j^4\right) \tag{11}$$

where subscript "sect" is used to distinguish from subscript "j", the value of each shell and $x = r$, because of the circular log shape. The calculation of $\mathrm{MOR}_{\mathrm{sect}}$ assumes, in principle, that we know the distribution of bending stress across the stem section, $\sigma(x)$, when $\mathrm{MOR}_{\mathrm{sect}}$ is reached. In the absence of this information, and based on $\sigma(x)$ of dry timber as its cross section reaches MOR (Kollmann 1968), we use two approaches (linear strain method and scaled MOR method) to calculate $\mathrm{MOR}_{\mathrm{sect}}$. The linear strain method applies a linear increase in ε from pith to bark, with a gradient governed by ε at MOR for the cylindrical shell at a radial distance of $\kappa_1 x_n$, where κ_1 is a factor between 0 and 1:

$$\mathrm{MOR}(z)_{\mathrm{sect}} = \frac{\gamma_{\mathrm{MOR},1}}{x_n(z)^3} \sum_{j=1}^{n} \sigma(\varepsilon, x(z), \kappa_1)_j \left(x(z)_{j+1}^3 - x(z)_j^3\right) \tag{12}$$

In our study, $\sigma(\varepsilon,x)$ in Equation 12 is the the average curve for Norway spruce and silver fir. The scaled MOR method simply applies a scaling of MOR:

$$\mathrm{MOR}(z)_{\mathrm{sect}} = \frac{\gamma_{\mathrm{MOR},2}}{x_n(z)^3} \sum_{j=1}^{n} \mathrm{MOR}(z,x)_j B(\kappa_2) \left(x(z)_{j+1}^3 - x(z)_j^3\right) \tag{13}$$

where $B(\kappa_2)$ is the degree of exploitation of MOR_j, represented as an array of n elements that increases from 0 to 1 between $x = 0$ and $x = \kappa_2 x_n$ and then remains constant, at a value of 1, between $x = \kappa_2 x_n$ and x_n. Parameters κ_1 and κ_2 thus govern the degree of plasticity of the outer part of the woody stem section.

In applying Equations 11–13 as linear regression models versus the experimental data for MOR and MOE for all the logs, the best fits yielded the values of parameters γ_{MOE}, $\gamma_{\mathrm{MOR},1}$, $\gamma_{\mathrm{MOR},2}$, κ_1 and κ_2. The regression coefficients of Equations 9 and 10 were checked, except for a_2 in Equation 9, by fitting them with the measured $\mathrm{RW}(r)$, $Q(r)$, MOE and MOR of the 20 logs in unconstrained nonlinear optimization (Matlab) and setting all $\gamma = 1.0$. The significance of the new coefficients was verified with the S-Plus 2000 software program (Insightful, Seattle, WA).

Results

Failure mechanisms and stress–strain curve characteristics

Bending failure usually began with buckling of the outermost wood fibers on the compression side of the log, followed by the outermost wood fibers on the tension side tearing apart (Table 4). The logs from the lower part of the Norway spruce trees, however, broke suddenly in the outer heartwood as a result of longitudinal shearing. For the three logs that did not fail

completely, i.e., fall apart, the applied force remained almost constant between half and maximum deflection, ending with a slight decrease.

The curves of bending stress–strain of the 20 logs were similar, with a quasi ideal-elastic first part to about two-thirds of MOR, from where the deformation increased significantly (Figure 2A). Close examination showed that both MOE and MOR generally decreased with stem height (Figures 2B and 3). Norway spruce logs were slightly stiffer but slightly weaker than silver fir logs (Figure 2C, Table 5). A comparison of the shapes of individual stress–strain curves (Figure 2A) and the types of failure (Table 4) revealed no obvious pattern. When MOE was defined as the first linear part of the stress–strain curve ($E(\varepsilon_E)_{LIN}$) instead of as 0.4MOR ($E(\varepsilon_E)_{0.4MOR}$), MOE was overestimated by 2.2%, on average, but the difference varied between 14% and −9.5%. When MOR was reached, the calculated shear stress $\tau(z,x)$ (Equation 4) was well below the estimated shear strength $\tau_{max}(z,x)$ (Equations 5 and 6) in the outer heartwood (Figure 4). Their ratio $\tau(z,x)/\tau_{max}(z,x)$ was highest in the pith at the thinner end of the log. Higher maximum ratios were generally found for logs from the lower part of the stem (e.g., 0.74 for Log 1 of Tree 7) than from the higher part of the stem (e.g., 0.34 for Log 4 of Tree 6). There was a trend of increasing MOR with increasing MOE, but the correlation was weak ($R = 0.30$).

The idealized stress–strain curves (example in Figure 2C) and η (cf. Equation 8) display some general tendencies. Averaged per tree height, mean $\varepsilon_{el\text{-}pl}$ and mean ε_{MOR} were 10% higher for silver fir than for Norway spruce, whereas mean $\alpha_{el\text{-}pl}$ and mean η differed by less than 1% between species. These variables increased with tree height, except for $\varepsilon_{el\text{-}pl}$, which remained nearly constant. Further, $\alpha_{el\text{-}pl}$ was equal to $0.28\eta + 0.73$ ($R^2 = 0.75$) for all logs combined. Although differences in mean values of the bending parameters were found between silver fir and Norway spruce, and according to stem height, none were significant (Table 6).

Table 4. Subsequent failure mechanisms (separated by a slash) observed during bending tests of 20 logs of silver fir (*Abies alba*) and Norway spruce (*Picea abies*). Failure mechanisms: c = wood fibers buckling on the compression side of the log; t = wood fibers tearing apart on the tension side; and s = longitudinal-cylindrical shearing. Listed are the clearly visible and significant mechanisms (naturally, the s-mechanism initiates within a brief moment of c- and t-failure).

Tree	Log 1	Log 2	Log 3	Log 4
Silver fir				
1	c[1]	t	c[1]	–
2	c / t	c / t	c / t	–
3	c / t	c / t	c / t	–
4	c / t	c[1]	–	–
Norway spruce				
5	s	c / s	c / t	–
6	s	t	c / t	c / t
7	s	c / s	–	–

[1] No complete failure.

The work absorbed by the mid-span of the log, in terms of $\int\sigma(\varepsilon)\,d\varepsilon$, the integral of stress as a function of apparent strain up to MOR, averaged 0.25 N mm^{-2} (min = 0.21, max = 0.30 and SE = 0.02 N mm^{-2}). The W_{MOR} calculated as bending stress integrated over the log volume (cf. Appendix) differed from the actual W_{MOR} absorbed, i.e., Fs. The detailed method (Equations A1, A2 and A4) yielded, on average, 1% smaller W_{MOR}, with relative standard, minimum and maximum errors of 4, −9 and 6%, respectively. Overly low values were calculated for logs from the lower part of the stem, whereas overly high values were calculated for logs originating from the upper part of the stem. The approximate method (Equations A3 and A4) yielded, on average, 4% larger W_{MOR}, with relative standard, minimum and maximum errors of 4, −1 and 15%, re-

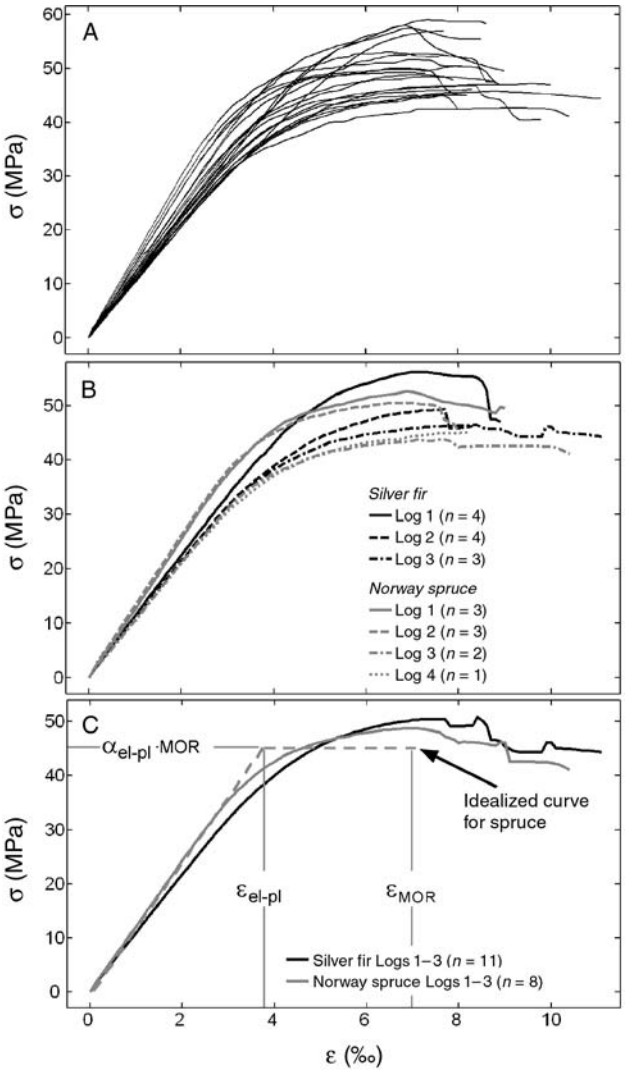

Figure 2. (A) Bending stress (σ) as a function of bending strain (ε) for all 20 logs from silver fir (*Abies alba*) and Norway spruce (*Picea abies*) trees. Mean $\sigma(\varepsilon)$ for logs grouped by (B) height and species and (C) by species. The idealized stress–strain curve in (C) is ideally elastic up to a percentage $\alpha_{el\text{-}pl}$ of the modulus of rupture (MOR), and ideally plastic between $\varepsilon_{el\text{-}pl}$ and ε_{MOR}.

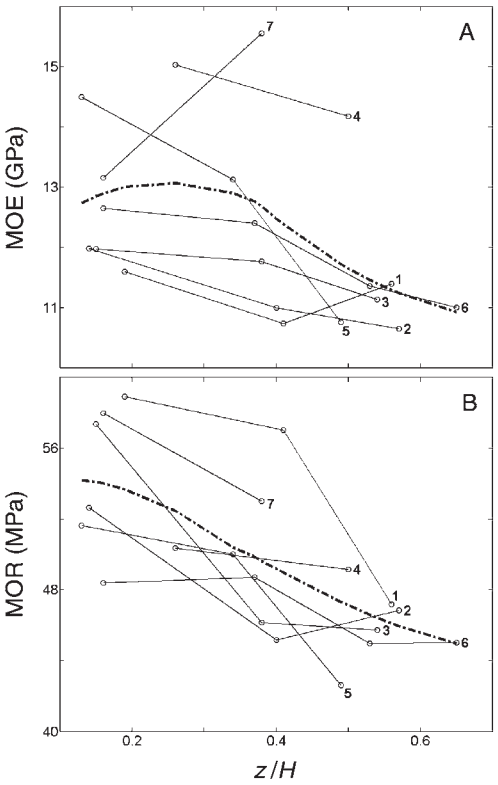

Figure 3. (A) Modulus of elasticity (MOE) and (B) modulus of rupture (MOR) of cross sections from silver fir (*Abies alba*) and Norway spruce (*Picea abies*) Trees 1–7 according to relative tree height = z/H (see Table 5 for numerical data). Dash-dot lines are smoothed averages of all trees (span = 95% of z/H range).

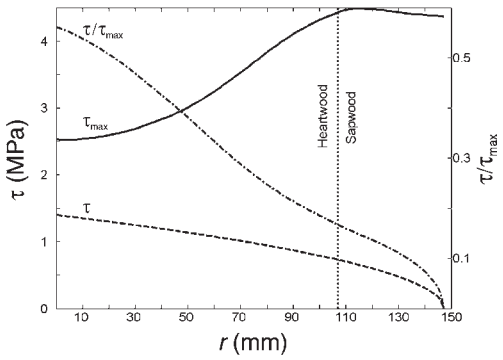

Figure 4. Shear stress (τ), shear resistance (τ_{max}) and their ratio as functions of radial distance from pith (r) in logs of silver fir (*Abies alba*) and Norway spruce (*Picea abies*) trees. Means are shown for all logs as MOR was reached and for the stem cross section where the highest ratios were found (below location of force application at the thinner side of the log). Shear failure occurred in the outer heartwood, i.e., about $60 < r < 100$ mm.

spectively, and a similar, but less clear, error distribution with stem height. When the detailed method was applied to a (fictive) three-point bending test of a beam with a square cross section and the same stress–strain curve data and in-span volume as our logs, W_{MOR}, and thus also W_{MOR}/V_0, were on average 20% smaller than the recorded W_{MOR}. The ratio W_{MOR}/V_0 ranged from 32 to 56, averaging 42 kN m m^{-3} (SE = 5 kN m m^{-3}), otherwise expressed as $W_{MOR} = 42V_0$ (W_{MOR} in kN m, V_0 in m^3) ($R^2 = 0.90$).

Table 5. Bending modulus of rupture (MOR) and modulus of elasticity (MOE) for Logs 1–4 of each silver fir (*Abies alba*) and Norway spruce (*Picea abies*) tree. The MOE is defined at 0.4MOR.

Tree	MOR (MPa)				MOE (GPa)			
	1	2	3	4	1	2	3	4
Silver fir								
1	58.9	57.0	47.2	–	11.6	10.7	11.4	–
2	52.7	45.2	46.9	–	12.0	11.0	10.6	–
3	57.4	46.2	45.8	–	12.0	11.8	11.1	–
Norway spruce								
4	50.4	49.2	–	–	15.0	14.2	–	–
5	51.6	50.0	42.6	–	14.5	13.1	10.8	–
6	48.4	48.7	45.0	45.0	12.6	12.4	11.4	11.0
7	58.0	53.0	–	–	13.2	15.6	–	–

Influences of analytical method on MOE, MOR and energy absorption

Approximation of the stem taper under bark as a truncated cone between the large- and small-end diameters of a log would yield non-negligible errors in diameter at the center of the log, especially in logs from the stem base where the curvature is strong. For all test trees, these errors were at the most 23, –6, –5 and –7 mm for Logs 1–4, respectively. The truncated cone approximation therefore resulted in relative errors in calculated values of MOE of –23, 8, 8 and 14%, and of MOR of –18, 6, 6 and 10% for Logs 1–4, respectively. The influence of the differences in diameter at the thin and the thick log ends (KL) on MOE was, however, low. Because KL was low for the tested logs (≤ 0.05), it reduced MOE by less than 0.13%. When shear deflections were considered (Equation 3), MOE increased by 3.3–7.4%. The self weight of the logs contributed, on average, 1.3% to MOR, but naturally did not contribute to MOE, because the addition of self weight does not change the initial slope of the stress–strain curve. The error in energy absorption, in terms of $\int\sigma(\varepsilon)\,d\varepsilon$, was at most –14%, when ignoring the precise stem taper and log weight.

Predictions of MOE and MOR

Because no significant differences in MOE or MOR were found between silver fir and Norway spruce, the prediction models were evaluated for all logs combined. Generally, MOE of the log section was well predicted by the models (Equations 9 and 11), unlike MOR (Equations 10, 12 and 13). The beneficial effect of the intact stem compared with separate cylindrical shells amounted to 6% for MOE. For MOR, this effect amounted to 0% when calculated with the linear strain method, and 9% when calculated with the scaled MOR method. The corresponding regression coefficients were

Table 6. Characteristics of the bending stress–strain and load-deflection curves for Logs 1–4 of each silver fir (*Abies alba*) and Norway spruce (*Picea abies*) tree. Abbreviations: ε_{el}, strain at 0.4MOR; $\varepsilon_{el\text{-}pl}$, strain at the break point between ideal elastic and ideal plastic bending; ε_{MOR}, strain at maximum load; $\alpha_{el\text{-}pl}$, proportion of MOR at plasticity; η, completeness of the material in bending (Equation 8); and MOR, modulus of rupture.

Tree	ε_{el} (‰)				$\varepsilon_{el\text{-}pl}$ (‰)				ε_{MOR} (‰)				$\alpha_{el\text{-}pl}$ (%)				η (%)			
	1	2	3	4	1	2	3	4	1	2	3	4	1	2	3	4	1	2	3	4
Silver fir																				
1	2.0	2.1	1.7	–	4.6	4.8	3.9	–	7.0	7.4	9.2	–	90	90	95	–	61	62	75	–
2	1.8	1.6	1.8	–	4.0	3.8	4.1	–	6.7	7.4	8.1	–	92	92	93	–	65	69	70	–
3	1.9	1.6	1.6	–	4.4	3.7	3.8	–	6.5	7.9	8.4	–	91	95	92	–	61	73	72	–
4	1.3	1.4	–	–	3.2	3.3	–	–	7.5	6.2	–	–	94	94	–	–	75	70	–	–
Norway spruce																				
5	1.4	1.5	1.6	–	3.3	3.6	3.7	–	6.6	6.6	8.5	–	92	94	94	–	71	69	74	–
6	1.5	1.6	1.6	1.6	3.5	3.6	3.7	3.7	6.9	6.6	6.6	7.9	92	92	92	92	69	68	68	71
7	1.8	1.4	–	–	4.0	3.2	–	–	6.5	6.3	–	–	91	92	–	–	64	70	–	–

$\gamma_{MOE} = 1.06$ ($R^2 = 0.93$, SE(MOE) = 0.16 GPa; cf. Equation 11), $\gamma_{MOR,1} = 1.00$ and $\kappa_1 = 0.90$ ($R^2 = 0.39$, SE(MOR) = 4.2 MPa; cf. Equation 12), and $\gamma_{MOR,2} = 1.09$ and $\kappa_2 = 0.85$ ($R^2 = 0.26$, SE(MOR) = 4.6 MPa; cf. Equation 13). When the measured cross-sectional modules were refitted with the measured RW(r) and $Q(r)$, we obtained the following statistical data for MOE: $\bar{a}$ = [–4098 –22.3 15749], $\bar{\boldsymbol{a}}$ = [–0.49 –0.25], R^2 = 0.95, SE(MOE) = 0.11 GPa; and for MOR: $\bar{a}$ = [–6.88 –45.2 68.2], $\bar{\boldsymbol{a}}$ = [–0.26 –0.89], $R^2 = 0.64$, SE(MOR) = 2.9 MPa, when using the scaled MOR method, $\gamma_{MOR,2} = 1.0$, and κ_2 = 0.85; and $\bar{\boldsymbol{a}}$ = [–0.35 –0.79], $R^2 = 0.64$, when refitting with the linear strain method, $\gamma_{MOR,1} = 1.00$, and $\kappa_1 = 0.90$. All $\bar{a}$ coefficients were highly significant ($P < 0.005$) except a_1 of MOR (P = 0.01). The initial and refitted regression models of MOE were similar, but measured MOR was more strongly influenced by $Q(r)$ than was predicted by Equation 9.

The predictions demonstrate a change in cross-sectional MOE with stem size and cambial age (Figures 5A and 5B): from a younger (0–25 years) to an older (> 60 years) stage, MOE increases by up to 60% for individual sections and by 35% on average. This trend is also apparent for MOR(z,r) predicted with the initial regression model but is less clear for the refitted model (Figure 5C). For both models, this increasing trend in MOR(z,r) with radius, was stronger in the lower stem. In the higher part, it was nonexistent for the initial model and slightly negative for the refitted model. Figure 5, which includes all logs and thus all stem heights admixed, shows that differences in MOE(z,r) and MOR(z,r) were greater among trees at the same height than among stem heights.

Discussion

Failure mechanisms and stress–strain curve characteristics

Fifteen of the 20 logs tested failed in the same way as sawn wood. The remaining five logs, from the lower part of Norway spruce trees broke because of longitudinal shearing apparently in the outer heartwood. The reasons for this difference in mode of breakage are unclear. The calculated maximum shear stresses were well below the estimated shear strengths (Figure 4). We postulate that there were local unobserved differences in radial growth properties, implying that local, strong radial gradients in strength and stiffness initiate slip along the grain, resulting in shear stresses that exceed the local shear strength. Heartwood fulfills an important function (cf. Stokes et al. 2001) in transmitting forces perpendicular to the stem into stress along the grain in the sapwood, which has a large capacity to absorb such stress. This function may, however, constitute a weak mechanical link, as found in 25% of our tests. It will be challenging to determine under what conditions this transmission function of heartwood is optimized.

We found no literature on the shape of the bending stress–strain curves of fresh tree stems. The curve shapes for the two species studied here were similar. This may have a natural explanation. Both species had similar annual ring widths and knottiness, both of which significantly influence the mechanical properties of bending (cf. Equations 9 and 10). Based on a comparison of the shapes of our bending stress–strain curves with those obtained from square specimens from the fresh heartwood and sapwood of Norway spruce (Lundström et al. 2007), it appears that the strain values are generally about 40% lower for the logs than for square specimens. It is probable that this difference is associated with the greater knottiness of the test logs, but it may also reflect an inherent behavior of the intact stem while bending.

Several important mechanical properties related to bending can be deduced from the stress–strain curves. The cross-sectional MOE values of the 90-year-old dominant and codominant Norway spruce test trees are: 50% higher than those of dominant Norway spruce of half the age at the same relative stem height (Brüchert et al. 2000); 70% higher than those of Sitka spruce of a third the age and with about the same dry stem bulk density (Cannell and Morgan 1987); and two to six times higher than those of 22-year-old Sitka spruce (Milne and Blackburn 1989). It is unlikely that the different methods of assessing stress and strain in the stem are the only reasons for these considerable differences. The stem normally produces stiffer wood at a mature stage, especially in the lower stem,

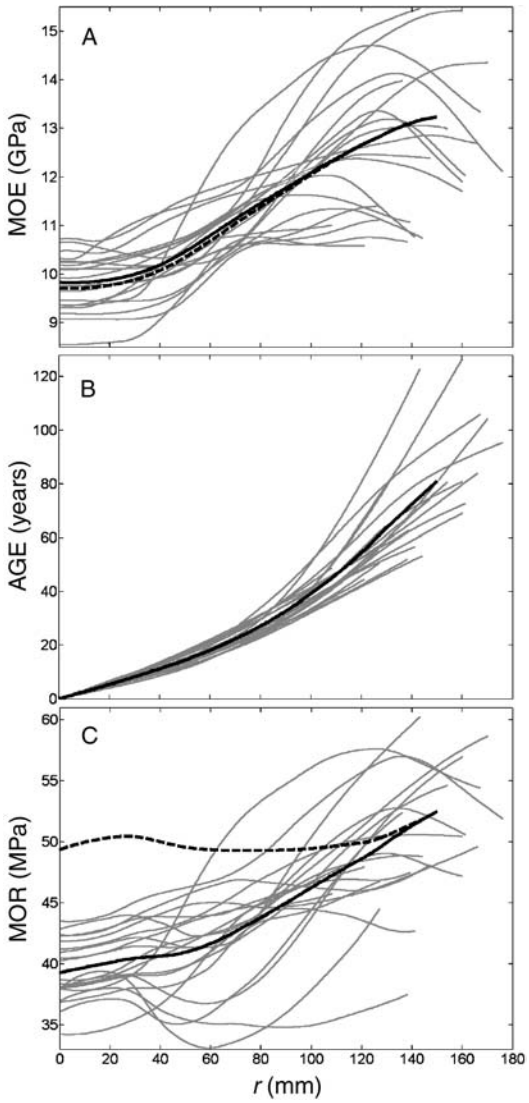

Figure 5. Modeled changes in (A) modulus of elasticity (MOE) and (C) modulus of rupture (MOR) of the cross section, with stem radius (r) and (B) cambial age at 1.3 m stem height (AGE). (A and C) Gray lines show the predicted MOE and MOR for all 20 logs (Equations 9–10 with the initial regression coefficients); solid black lines are means up to $r = 150$ mm, resulting from the initial coefficients; and dashed black lines are means resulting from the refitted coefficients. (B) Gray lines represent individual logs, and the black line is the mean.

which then influences the overall stiffness of the stem (cf. Figures 3A and 5A; Lundström et al. (2007)).

The cross-sectional MOR values can be compared with the mean value of 55 MPa obtained at a stem height of 2.5 m for 73, 100-year-old, Scots pine trees, which had grown more slowly at latitude 61° N in Sweden than our test trees (S. Brüzelius, Rundvirke Poles AB, personal communication). The logs we tested displayed a greater decrease in MOR with tree height (Figure 3B) than found by Lundström et al. (2007). This difference may be associated with a comparatively greater increase in knottiness in the outer part of the stem above a relative tree height of 0.3 among the logs we studied.

There have been few studies on W_{MOR} for fresh intact stems. Expressing W_{MOR} in terms of $\int\sigma(\varepsilon)\,d\varepsilon$ facilitates comparisons of W_{MOR}, because comparisons of W_{MOR} calculated as load times deflection assume an identical geometry of load application and cross section. We found that W_{MOR} was 20% lower in the three-point than in the four-point bending tests, as a result of the smaller stem volume subjected to stress in the former. If $\int\sigma(\varepsilon)\,d\varepsilon$ and bending moment along the log are known, the work effectively absorbed by a log, or any type of member subject to bending, can also be calculated (Equations A1–A4). In our case, W_{MOR} calculated by the detailed $\int\sigma(\varepsilon)\,d\varepsilon$-method (Equations A1, A2 and A4) yielded relatively small errors compared with the work effectively absorbed, i.e., the measured force times deflection. Thus, this method appears useful for estimating work absorbed by a tree stem subject to bending. The errors in calculated W_{MOR} may arise because of differences between the actual (not exactly known) and the assumed: (1) cross-sectional distribution of bending or shearing stress with stem height; and (2) bending moment along the log. The approximate $\int\sigma(\varepsilon)\,d\varepsilon$-method (Equations 16 and 17) also appears useful, although it tends to overestimate the absorbed energy, because the radial difference in MOR is not considered. The mean value of $\int\sigma(\varepsilon)\,d\varepsilon$ up to MOR of the logs (0.25 N mm^{-2}) is lower than the values of 0.40 and 0.61 N mm^{-2} obtained for specimens from the heartwood and sapwood of fresh Norway spruce by Lundström et al. (2007). This difference is due to the compressed stress–strain curves in the strain direction for the logs, as discussed previously. It is clear that intact stems and sawn wood display different behaviors while bending. It is also apparent that the bending properties of living stems largely depend on the growth conditions experienced by the tree. The growth pattern of the Norway spruce and silver fir stems in our study is representative of other sites with similar climatic conditions in and around the Alps (Schweingruber 1996). However, stems of the same species grown under different conditions will exhibit different bending properties to those observed here.

Influences of test and analysis methods

Stem bending stress and strain can be assessed and interpreted in various ways. In laboratory tests, such as four-point, three-point and cantilever bending, curves of bending stress–strain can be obtained for stem sections taken from different tree heights under controlled and close to standardized conditions (DIN 2000, BSI 2001, CEN 2003). A drawback is that the longitudinal growth stresses within the stem of a standing tree (Fourcaud et al. 2003, Huang et al. 2005) are released when the tree is felled. However, these stresses represent only a few percent of the stem bending resistance for Norway spruce and silver fir (Dinwoodie 2000), and the internal growth stresses may, at least theoretically, be superimposed on the bending stress obtained in the laboratory test. The stress– strain of the stem while bending can also be assessed in situ, by pulling the stem of a standing tree sideways (cf. Milne and Blackburn 1989), but it may then be more difficult to precisely assess strains and load application along the stem. For any test used, our investigations show that a precise measurement of stem

taper is especially important. Otherwise errors of more than 20% may arise in the calculated stress–strain and the derived bending properties, making comparisons of results from different investigations less meaningful (cf. Morgan and Cannell 1994). In addition to bending, the stem of a standing tree can occasionally be subject to torsion (e.g., if the crown is asymmetric) and length forces that may impair the bending capacity of the stem. Torsion is, however, rare, and length forces are of low magnitude (Mayer 1985, Amtmann 1986), so neither were considered in this study.

Predictions of cross-sectional MOE and MOR

The method used for predicting MOE appears to be robust. The predictions of MOR were only approximate because of several failure mechanisms that are difficult to predict. The small differences in error between the two methods of predicting MOR (Equations 12 and 13) are irrelevant in the context of the study, but Equation 13 has the advantage of being simpler. The MOR(r) values predicted with the initial and with the refitted regression coefficient differed. Although it is not evident which method best predicts MOR(r), the tested MOR($r = D_0/2$) is predicted better with the refitted version. The method to obtain the regression coefficients of the refitted version statistically weights the RW and Q in the outermost part of the stem cross section heavily. Also, the prediction using the initial regression coefficients is statistically stronger for the mean of MOR(r) than for individual MOR(r)s because of the statistical effect of linear transformation. The increasing trend in this initial mean MOR(r) with radius, and thus with the cambial age, as well as the strong correlations between MOE and MOR for wood in general (Kollmann 1968) suggest that MOR should increase with cambial age, similarly to MOE. For better predictions of cross-sectional MOR, we need to know more about the stem-bending failure mechanisms in trees differing in age and radial stem growth properties.

Acknowledgments

We are indebted to the Board of the Swiss Federal Institutes of Technology for financial support for this work, conducted within the project "Tree Stability and Natural Hazards." We thank the Institute of Structural Engineering at the ETHZ for the use of their laboratory, Hanspeter Arm for his precise experimental work, and Silvia Dingwall for revision of the text.

References

Adjanohoun, G., J.-L. Guillot, J.-D. Lanvin and R. Cholat. 1998. Small roundwood grading by nondestructive x-rays and ultrasonic waves methods. 5th World Conf. on Timber Engineering. Presses Polytechniques et Universitaires Romandes, Lausanne, Switzerland. www.ndt.net/article/v04n11/adjanoh/adjanoh.htm.

Amtmann, R., 1986. Dynamische Windbelastung von Nadelbäumen. Forstl. Forsch. Ber. 74:215.

Brüchert, F., G. Becker and T. Speck. 2000. The mechanics of Norway spruce (*Picea abies* (L.) Karst): mechanical properties of standing trees from different thinning regimes. For. Ecol. Manage. 135:45–62.

BSI. 2001. Timber poles for overhead lines—test methods—determination of modulus of elasticity, bending strength, density and moisture content. BS EN 12509 2001. BSI, London, 14 p.

Cannell, M.G.R. and J. Morgan. 1987. Young's modulus of sections of living branches and tree trunks. Tree Physiol. 3:355–364.

CEN. 2003. EN 408: Timber structures—structural and glued laminated timber—determination of some physical and mechanical properties. Brussels, 12 p.

DIN. 1992. Normen über Holz. Deutsches Institut für Normung. DIN-Taschenbuch Vol. 31. 6th Edn. Beuth, Berlin, Köln, 260 p.

DIN. 2000. Normen über Holz. Deutsches Institut für Normung. DIN-Taschenbuch Vol. 31. 7th Edn. Beuth, Berlin, Köln, 597 p.

Dinwoodie, J.M. 2000. Timber: its nature and behaviour. 2nd Edn. E&FN SPON, London, 257 p.

Einspahr, D.W., R.H. Vaneperen and M.L. Fiscus. 1984. Morphological and bark strength characteristics important to wood–bark adhesion in hardwoods. Wood Fiber Sci. 16:339–348.

Fourcaud, T., F. Blaise, P. Lac, P. Castera and P. de Reffye. 2003. Numerical modeling of shape regulation and growth stresses in trees II. Implementation in the AMAPpara software and simulation of tree growth. Trees 17:31–39.

Green, D.W., J.E. Winandy and D.E. Kretschmann. 1999. Mechanical properties of wood. USDA For. Serv., Forest Products Lab., Madison, WI. www.fpl.fs.fed.us/documnts/fplgtr/fplgtr113/ch04.pdf.

Huang, Y.S., S.S. Chen, L.L. Kuo-Huang and C.M. Lee. 2005. Growth strain in the trunk and branches of *Chamaecyparis formosensis* and its influence on tree form. Tree Physiol. 25:1119–1126.

Kollmann, F.F.P. 1968. Principles of wood science and technology. Solid wood. Vol. 1. Springer-Verlag, Berlin, 592 p.

Kucera, L.J. and B. Gfeller. 1994. Einheimische und fremdländische Nutzhölzer. Professur Holzwissenschaften, ETHZ, Zurich, 144 p.

Laasasenaho, J., T. Melkas and S. Alden. 2005. Modeling bark thickness of *Picea abies* with taper curves. For. Ecol. Manage. 206: 35–47.

Lundström, T., U. Heiz, M. Stoffel and V. Stöckli. 2007. Fresh-wood bending: linking the mechanical and growth properties of a Norway spruce stem. Tree Physiol. 27:1229–1241.

Mattheck, C. and H. Breloer. 1994. The body language of trees: a handbook for failure analysis. HMSO, London, 240 p.

Mayer, H. 1985. Baumschwingungen und Sturmgefährdung des Waldes. Universität München, Meteorologisches Institut, München, 51, 247 p.

Milne, R. and P. Blackburn. 1989. The elasticity and vertical distribution of stress within stems of *Picea sitchensis*. Tree Physiol. 5: 195–205.

Morgan, J. and M.G.R. Cannell. 1994. Shape of tree stems—a reexamination of the uniform stress hypothesis. Tree Physiol. 14:49–62.

Newlin, J.A. and G.W. Trayer. 1956. Deflection of beams with special reference to shear deformations. USDA For. Serv., Forest Products Lab., Report 1309, Madison, WI, 18 p.

Schmidt-Vogt, H. 1991. Die Fichte: ein Handbuch in zwei Bänden. Waldbau, Ökologie, Urwald, Wirtschaftswald, Ernährung, Düngung, Ausblick Vol. 2/3. Verlag Paul Parey, Hamburg und Berlin, 781 p.

Schweingruber, F.H. 1996. Tree rings and environment. Dendroecology. Haupt, Bern, 609 p.

SIA. 2003. Timber structures—supplementary specifications. Schweizerischer Ingenieur- und Architektenverein (SIA), Zurich, 265/1, 27 p.

Stokes, A., T. Fourcaud and S. Berthier. 2001. How trees stand up and fall down: tree resistance to wind, or strange things that happen under stress. Int. Conf. Tree Structure and Mechanics, Savannah, GA, pp 21–37.

Trendelenburg, R. and H. Mayer-Wegelin. 1955. Das Holz als Rohstoff. 2nd Edn. J.F. Lehmanns Verlag, Munich, 541 p.

USDA. 1972. The moisture content and specific gravity of the bark and wood of northern pulpwood species. USDA For. Serv., North Central Forest Exp. Stn., Minnesota, Res. Note NC-141, 3 p.

Appendix

Table A1. List of symbols and notations and their definitions and units used in the study.

Symbol/Notation	Description	Unit
AGE	Cambial age counted from pith	year
D, D_0; $_{1, 2, c}$	Stem diameter on and under bark; reference to thin and thick log end and to log centre	mm, m
A_0	Cross-sectional area of woody log	mm^2, m^2
E; E_F	Secant modulus of elasticity due to pure bending, i.e., elasticity corrected for shear deformation = σ/ε_E; $E_F = \sigma_F/\varepsilon_F$	GPa
ε; ε_E; ε_F	Apparent bending strain (simply "bending strain"); ε corrected for shear deformation; ε due to F and corrected for shear deformation	–
ε_{el}; ε_{MOR}	ε as σ reaches: 0.4MOR (defined limit of elasticity); and MOR	–
$\varepsilon_{el\text{-}pl}$, $\alpha_{el\text{-}pl}$	The ideal elastic–ideal plastic $\sigma(\varepsilon)$-curve has a break point at $\varepsilon = \varepsilon_{el\text{-}pl}$ and $\sigma = \alpha_{el\text{-}pl}$MOR	–
F; F_{max}; F_g	Applied force in bending test; maximum applied F; concentrated (fictive) force causing same deflection as log weight	N
g; $_g$	Earth gravity; reference to own weight	$m\ s^{-2}$
G	Shear modulus in the z-direction, i.e., along fibers	MPa
γ_{MOE}; $\gamma_{MOR,1}$; $\gamma_{MOR,2}$	Coefficients accounting for the beneficial effect on MOE and MOR of intact logs compared to sawn wood (cf. Equations 11–13)	–
η	Completeness of the material in bending (cf. Equation 8)	–
H	Total tree height	m
K	Log taper = $(D_{02} - D_{01})/(D_{01}L)$	m^{-1}
κ_1; κ_2	Coefficients of plastification (cf. Equations 12 and 13)	–
L_{tot}; L; L_F	Test log length (total; in-span); and distance between support and force application	mm, m
MOE	Modulus of elasticity = the secant modulus of $\sigma(\varepsilon)$ as 0.4MOR is reached	GPa
MOR	Modulus of rupture = maximum value of $\sigma(\varepsilon)$	MPa
$\int\sigma(\varepsilon)d\varepsilon$	Integration of $\sigma(\varepsilon)$ up to σ = MOR, i.e., area under $\sigma(\varepsilon)$-curve	MPa
Q; $Q(r)$	Knottiness: of the stem cross section; and at the radial distance (r) from the pith (cf. Equation 1)	–
r; r_0	Radial coordinate of the stem, ranging from the stem center ($r = 0$) to the bark ($r = r_0$)	mm, m
ρ_w, ρ_b; ρ_0	Density of fresh wood and of bark; calculated dry wood density	$kg\ m^{-3}$
RW	Annual ring width	mm
σ; σ_F; σ_g	Bending stress; σ due to F; σ due to weight of log	MPa
I_{0c}	Moment of inertia about the log center	mm^4, m^4
s; $s_{F_{max}}$; s_g	Mid-span deflection of log; s at F_{max}; s due to weight of log	mm, m
τ, τ_{max}	Shear stress and resistance in z-direction	MPa
u	Wood moisture content = mass of water/oven-dry mass	%
V_0	Volume of woody log within the bending span	m^3
W; W_{MOR}; $W_{F_{max}}$	Work absorbed in bending; W at MOR; W due to F_{max}	N m
x, y, z	Cartesian coordinates of standing tree stem: z is height above stem base; and x is in the direction of deflection, $x = 0$ at stem center	mm, m
ϕ	Rotation around z-axis	rad

Work absorbed in bending, based on bending stress as a function of bending strain

The total work absorbed by a member subjected to bending can be expressed as the sum of energies absorbed by the small volume elements of the member. Below, this is exemplified at two levels of detail for the round logs that we tested.

The bending work absorbed within an infinitesimally thin slice of the middle cross section of the log (i.e., the test section) can be expressed as:

$$\frac{dW}{dz'}(z'_{test})_{sect} = \int_{-r_0}^{r_0}\left(\int_0^{\varepsilon(x)}\sigma(\varepsilon,x)\,d\varepsilon\right)C(x)\underbrace{2y(x)\,dx}_{dA_y(x)} \qquad (A1)$$

where: $0 < z' < L$ is the coordinate along the log subjected to bending and $z'_{test} = L/2$; r_0 is the radius of the middle of the woody log; $\sigma(\varepsilon,x)$ is the bending stress as a function of bending strain and distance from the log centre; $dA_y(x)$ is an area segment of the cross section (cf. Figure A1) with an infinitesi-

mal height dx, so that the strain occasioned by the bending can be assumed to be constant within the segment; and $C(x)$ is a coefficient that accounts for the radial gradient in MOR across the circular log:

$$C(x) = \frac{\sum_{i=1}^{n} dA_{xy}(x)_i \, \mathrm{MOR}(x)_i}{dA_y(x) \, \mathrm{MOR}_{\mathrm{sect}}} \gamma_{\mathrm{MOR}} \quad \text{(A2)}$$

where γ_{MOR} = 1.09 or 1.00 (found in this study), depending on

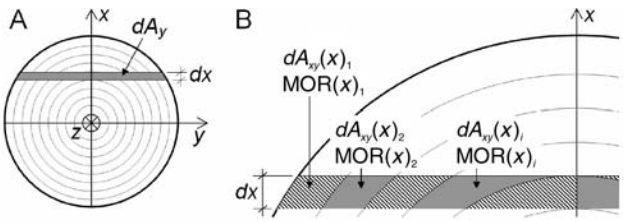

Figure A1. (A) Log cross section with schematic, enlarged annual year rings. Axes: z is the height above the stem base, and y the axis of applied bending moment in the tests, which causes deflections in the x-direction. (B) Enlargement of the upper left part of (A). Modulus of rupture (MOR) of each area element dA_y is calculated (Equation 15) on the basis of $\mathrm{MOR}(x)_i$ of finite area elements $dA_{xy}(x)_i$.

the x-wise distribution of bending stress (Equation 12 or 13). The other notations are explained in Figure A1B. If the distribution of bending stress across the section is approximated as triangular, then Equation A1 simplifies to:

$$\frac{dW}{dz'}(z'_{\mathrm{test}})_{\mathrm{sect}} = \tfrac{1}{4}\pi r_0^2 \int_0^{\varepsilon(r_0)} \sigma(\varepsilon)\, d\varepsilon \quad \text{(A3)}$$

This seems justified if: (1) the bending remains elastic, or at least, does not cause bending strain larger than that at MOR (cf. Table 6); and (2) the variation in $\mathrm{MOR}(r)$ is low. The work absorption along the log is proportional to the applied bending moment $M(z')$, which is obtained from basic mechanics. Therefore, the total bending work W absorbed by the log can be expressed as:

$$W = \int_0^L \frac{dW}{dz}(z'_{\mathrm{test}})_{\mathrm{sect}} \frac{M(z')}{M(z'_{\mathrm{test}})} dz' \quad \text{(A4)}$$

Consequently, the total work absorbed by a log can be calculated if data are available on: (1) the curve of the bending stress–strain, which may or may not be linear, of one stem section; (2) the shape or radius of this cross section; (3) the radial variation of MOR across the section; and (4) the applied bending moment along the log.